

# Silicene on Ag(111) : domains and local defects of the observed superstructures

Haik Jamgotchian<sup>1</sup>, Yann Colignon<sup>2</sup>, Bénédicte Ealet<sup>1</sup>, Bence Parditka<sup>2,3</sup>, Jean-Yves. Hoarau<sup>1</sup>, Christophe Girardeaux<sup>2</sup>, Bernard Aufray<sup>1,a</sup> and Jean-Paul. Bibérian<sup>1</sup>

<sup>1</sup> Aix-Marseille Université, CNRS, CINaM, UMR 7325, 13288 Marseille, France

<sup>2</sup> Aix-Marseille Université, CNRS, IM2NP, UMR 7334, 13397 Marseille, France

<sup>3</sup> Department of Solid State Physics, University of Debrecen, H-4026 Debrecen, Bem ter 18/b., Hungary

E-mail: <sup>a</sup>aufray@cinam.univ-mrs.fr

**Abstract.** On Ag(111) substrate, the growth of a silicene layer (the equivalent of graphene for silicon) gives rise to four main superstructures due to the epitaxy between the silicene layer (honeycomb structure) and the Ag(111) substrate. Depending on both the substrate temperature and the deposition rate, the following superstructures were observed:  $(4 \times 4)$ ,  $(\sqrt{13} \times \sqrt{13})R13.9^\circ$ ,  $(2\sqrt{3} \times 2\sqrt{3})R30^\circ$  and  $(\sqrt{7} \times \sqrt{7})R19.1^\circ$ . Each one corresponds to a specific rotation of the silicene layer with respect to the silver substrate. In this paper we show and discuss for each superstructure all the expected equivalent domains due to the symmetry properties of both the silicene honeycomb structure and the trigonal silver surface. Finally, we show, from STM images of the  $(2\sqrt{3} \times 2\sqrt{3})R30^\circ$  superstructure, the role played by periodic local defects on the average direction of the superstructures.

## 1. Introduction

After the publication of three important papers showing a possible synthesis of silicene (graphene-like silicon monolayers) on the silver substrates (Ag(100)[1] Ag(110)[2] and Ag(111)[3] faces), many groups all around the world started to work on this system [4]. Recently and especially on the Ag(111) face, the growth of silicene layers has been confirmed even if, different atomic models were proposed [5, 6, 7, 8, 9, 10, 11, 12, 13, 14]. At least four superstructures have been observed and/or predicted due to the epitaxy between the silicene layer (honeycomb structure) and the Ag(111) substrate (trigonal structure). Depending on the substrate temperature and the deposition rate, different superstructures are observed. A  $(4 \times 4)$  superstructure is obtained if the substrate temperature is maintained between 150 and 180°C and with a relatively slow deposition rate (0.5 ML / h). A  $(2\sqrt{3} \times 2\sqrt{3})R30^\circ$  is obtained with a substrate temperature above 280°C and with a higher deposition rate (5 ML/h). In between these two experimental growth conditions, a mixture of these two superstructures plus a  $(\sqrt{13} \times \sqrt{13})R13.9^\circ$  superstructure is obtained. As expected, the  $(4 \times 4)$  superstructure is due to the perfect match between four silver inter-atomic distances (1,156 nm), and three silicon hexagons (1,152 nm), both structures oriented with the same [110] directions. We have previously shown that starting from the  $(4 \times 4)$  superstructure, a rotation  $\alpha$  of the silicene layer relatively to the silver substrate gives rise successively to a first  $(\sqrt{13} \times \sqrt{13})R13.9^\circ$



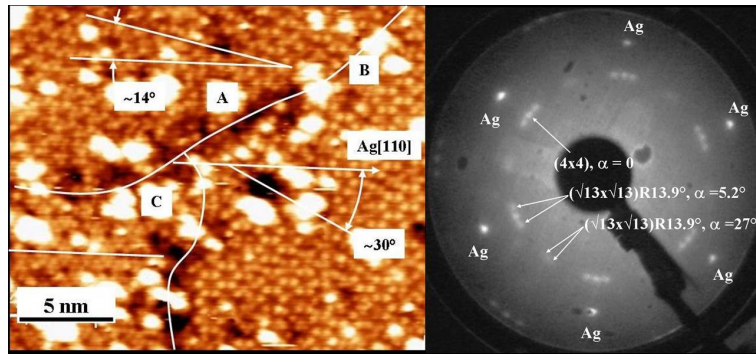


**Figure 1.** a) STM image of a mixture of superstructures. ( $V = -1.1V$ ,  $I = 1.2nA$ ) b) Corresponding LEED pattern showing:  $(\sqrt{13} \times \sqrt{13})R13.9^\circ$ , domain A,  $(2\sqrt{3} \times 2\sqrt{3})R30^\circ$ , domain B and  $(4 \times 4)$  domain C.

( $\alpha = 5.2^\circ$ ), a  $(2\sqrt{3} \times 2\sqrt{3})R30^\circ$  ( $\alpha = 10.9^\circ$ ), a  $(\sqrt{7} \times \sqrt{7})R19.1^\circ$  ( $\alpha = 19.1^\circ$ ), and finally a second  $(\sqrt{13} \times \sqrt{13})R13.9^\circ$  ( $\alpha = 27^\circ$ ) structure [6]. In this paper we show and discuss for each superstructure all the expected equivalent domains due to the symmetry properties of both the silicene honeycomb structure and the trigonal silver surface. Finally, we show from STM images of the  $(2\sqrt{3} \times 2\sqrt{3})R30^\circ$  superstructure, the role played by periodic local defects on the average direction of the superstructures.

## 2. The five main superstructures and their associated domains.

From a general point of view, the LEED pattern of a given superstructure, with respect to the substrate, reveals two important information: the first one is the over-periodicity (i.e. a length) and the second one is the orientation of the superstructure (i.e. a direction). As a consequence, when different superstructures are present simultaneously on the same surface, both information (periodicity and direction) are used in order to identify the different superstructures observed by Scanning Tunneling Microscopy (STM) [15]. When the silicene were grown on Ag(111) then we generally observed by STM and LEED the coexistence of different superstructures which are difficult to identify (see Figure 1 (a)). Since the silver sample is always in the same orientation before and after the silicene growth, we used the information extracted from LEED (direction and periodicity) to identify each superstructure. This is how we had shown [6], and later confirmed [11] that morphologies of the silicene layer reflects the position of each silicon atom with respect to the silver ones: in other words when a silicon atom is situated on top of a silver atom, it appears always higher than those located in threefold sites or in bridge positions, as shown schematically in figure 2. All the STM images, which are presented in this paper, have been obtained after the same experimental protocol explained in detail in [6].

## 3. The single domain $(4 \times 4)$ superstructure.

This superstructure is obtained thanks to the perfect match amongst four nearest neighbour silver distances (1.156nm) and three hexagonal cells of the (111) surface of silicon (1.152nm). Due to the superposition of both axes of symmetry between the silver and the silicene planes ( $\alpha = 0^\circ$ ), there is only one domain. As shown in figure 3, the ball model starting with hexagons of silicon atoms around a silver atom explains the STM image: the silicon atoms located close to the top position of silver atoms correspond to the intense spots of the STM image. DFT calculations have confirmed the first model, showing that the density of states is located around the silicon atoms [8].

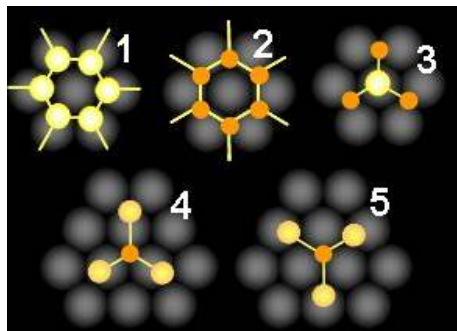


**Figure 2.** Ball models of adsorption sites of silicon on silver used to interpret all the STM images. 1) six silicon atoms close to top positions around a silver atom. 2) six silicon atoms close to three fold positions around a silver atom. 3) One silicon atom on top position and three silicon atoms in bridge positions. 4) One silicon atom in a three-fold site and three silicon atoms close to top positions. 5) Mirror image of 4)

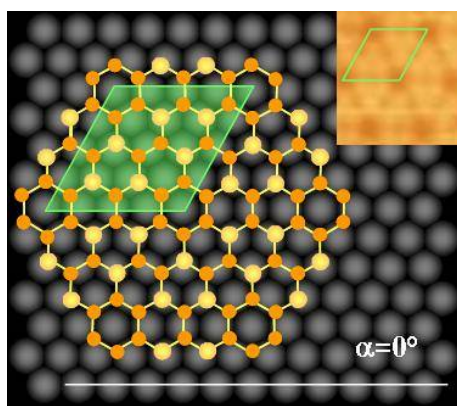


**Figure 3.** Ball models of the  $(4 \times 4)$  superstructure and the corresponding STM image.

#### 4. The two $(\sqrt{13} \times \sqrt{13})R13.9^\circ$ superstructures and four domains

The LEED pattern of the  $(\sqrt{13} \times \sqrt{13})R13.9^\circ$  shows two directions for the superstructure corresponding to two angles:  $\alpha = 5.2^\circ$ , and  $\alpha = 27^\circ$  as shown in figure 1 b. The corresponding STM image on figure 4 shows the two different  $(\sqrt{13} \times \sqrt{13})R13.9^\circ$  structures .

For:  $\alpha = 5.2^\circ$ , the superstructure not being on a silver axis of symmetry, there are two mirror domains rotated:  $+13.9^\circ$  and  $-13.9^\circ$  with respect to the Ag[110] direction. For the sake of simplicity, only one orientation:  $+13.9^\circ$  is discussed. The ball model and the corresponding STM image are shown in figure 5 a. Here again, the intense spots of the STM image correspond to silicon atoms located on top of silver atoms.

For:  $\alpha = 27^\circ$ , the superstructure corresponds to a mirror structure with respect to the Si[110] direction. For this structure there are also two domains rotated:  $+13.9^\circ$  and  $-13.9^\circ$  with respect to the Ag[110] direction. The ball model for  $+13.9^\circ$  and the corresponding STM image are shown in figure 5 b. Here there is no silicon atom on top of silver atoms. Instead, we observe intense areas corresponding to groups of silicon atoms.

Finally, there is a total of four domains for this superstructure. This is a unique case where the same superstructure  $(\sqrt{13} \times \sqrt{13})R13.9^\circ$  has two different atomic compositions in the unit cell. The LEED pattern corresponding to each one of these structures shows the same position of the diffraction spots, but with very different intensities (Figure 1 b). The intense spots of each of these superstructures correspond to the silicene unit cell: distance and angle between two silicon hexagons [15].

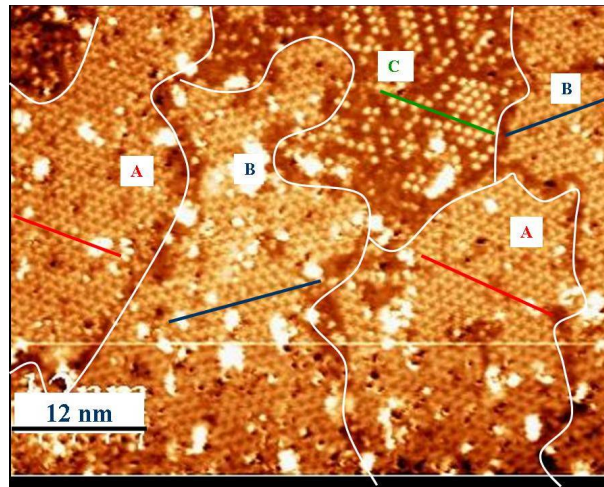


**Figure 4.** STM image showing a mixture of the two different  $(\sqrt{13} \times \sqrt{13})R13.9^\circ$  superstructures ( $V = -1.4V$ ,  $I = 800pA$ ). Domains A and B correspond to the same superstructures ( $\alpha = 5.2^\circ$  and  $\alpha = -5.2^\circ$  respectively). Domain C is the other type of superstructure ( $\alpha = 27^\circ$ ). All domains are separated by grain boundaries.

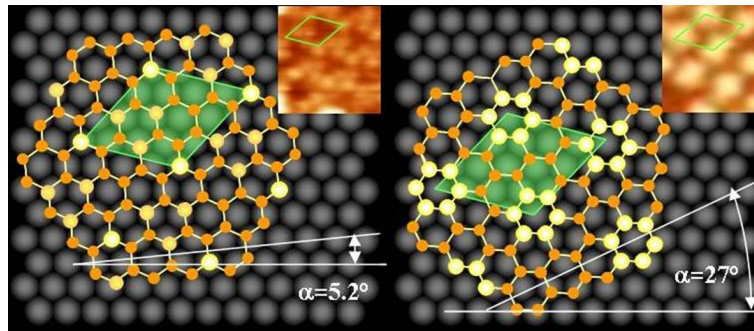


**Figure 5.** Ball model of the two different  $(\sqrt{13} \times \sqrt{13})R13.9^\circ$  superstructures with (a)  $\alpha = 5.2^\circ$  and (b)  $\alpha = 27^\circ$

### 5. The two domains $(2\sqrt{3} \times 2\sqrt{3})R30^\circ$ superstructure

This superstructure is obtained when the silicene layer is rotated by an angle,  $\alpha = 10.9^\circ$ , with respect of the silver substrate ( Figure 6 ). The direction of the  $(2\sqrt{3} \times 2\sqrt{3})R30^\circ$  superstructure is on a silver symmetry axis, so we expect only two domains due to the mirror structure with respect to the Si[110] direction as it is shown on the figure 6. The two domains exist on the Ag surface but cannot be separated by STM since they form the same protrusions structure as it is shown on the ball model of figure 6.

### 6. The two domains of the $(\sqrt{7} \times \sqrt{7})R19.1^\circ$ superstructure.

This superstructure was predicted [6] based on the good match between the silicene layer and the silver lattice. This superstructure has been later observed by Chiappe et al. [11]. The STM morphology shows big protrusions forming a trigonal network with the periodicity of 0.76 nm rotated  $19.1^\circ$  with respect to the Ag[110] direction. This superstructure not being on a silver axis of symmetry, two domains rotated  $19.1^\circ$  and  $-19.1^\circ$  are expected. As shown on figure 7,



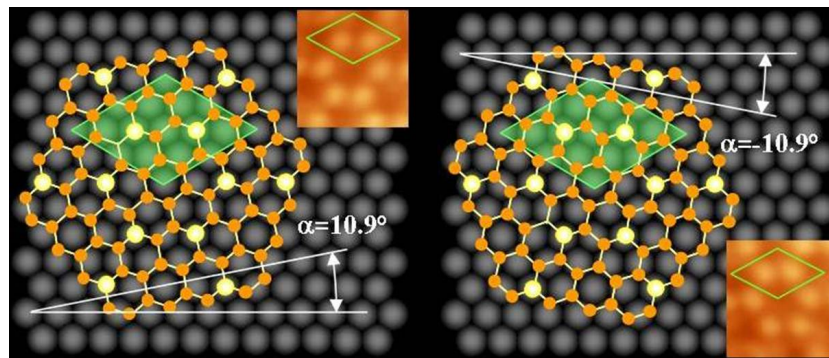


**Figure 6.** The two models of the  $(2\sqrt{3} \times 2\sqrt{3})R30^\circ$  superstructure: a)  $\alpha = +10.9^\circ$  b)  $\alpha = -10.9^\circ$

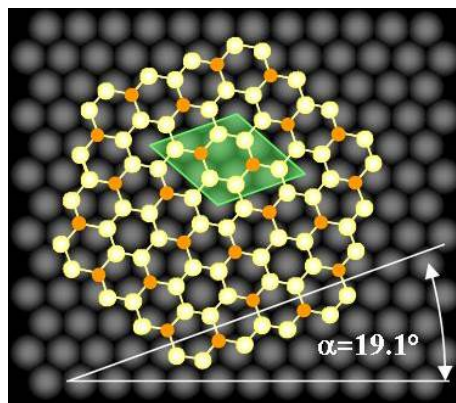


**Figure 7.** Ball model of the  $(\sqrt{7} \times \sqrt{7})R19.1^\circ$  superstructure

a model similar to the  $(\sqrt{13} \times \sqrt{13})R13.9^\circ$  superstructure with 6 silicon atoms around a silver atom is proposed. For this model also, three first silicon atoms are also situated close to the top of silver atoms giving rise to the big protrusion observed by STM [11].

## 7. Effects of local defects

As shown on the filled states STM images on figure 8, the direction of the  $(2\sqrt{3} \times 2\sqrt{3})R30^\circ$  superstructure is not exactly at an angle of  $30^\circ$ . This observation is explained by regular periodic defects formed around a perfect domain as it is highlighted on the figure 8, giving rise to the observed average slight rotation shift, in this case about  $4^\circ$ . The value of the rotation shift can change depending on the size of the  $(2\sqrt{3} \times 2\sqrt{3})R30^\circ$  domains: the larger the domains, the smaller the angle shifts. In addition, this analysis could also explain the Moiré pattern observed by Feng et al. [5].

Interestingly figure 9 shows two domains of  $(2\sqrt{3} \times 2\sqrt{3})R30^\circ$  with defects both close to  $30^\circ$  one rotationally shifted positively, and the other negatively, separated by a grain boundary. Each domain corresponds to a rotation of the silicene layer,  $\alpha = +10.9^\circ$  and  $\alpha = -10.9^\circ$ . The approximate  $7^\circ$  disorientation highlighted in figure 9 corresponds to approximately two times  $3.5^\circ$ : i.e.  $3.5^\circ$  for  $\alpha = +10.9^\circ$  and  $-3.5^\circ$  for  $\alpha = -10.9^\circ$ . When alpha is  $+10.9^\circ$  the local defects deform the structure towards the  $(\sqrt{13} \times \sqrt{13})R13.9^\circ$  structure with the silicene layer rotated by  $+5.2^\circ$ . Similarly when alpha is  $-10.9^\circ$  the local defects deform the structure towards the  $(\sqrt{13} \times \sqrt{13})R13.9^\circ$  structure with the silicene layer rotated by  $-5.2^\circ$ .

In this case local defects permits to distinguish the two different  $(2\sqrt{3} \times 2\sqrt{3})R30^\circ$  structures that are undistinguishable by STM as shown on the ball models of figure 6.

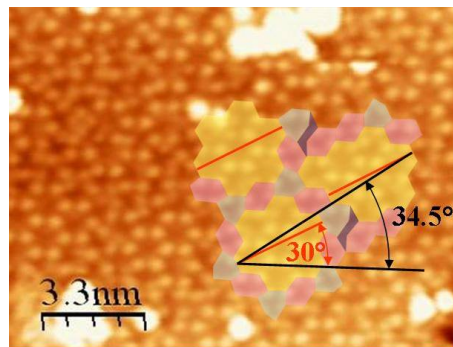


**Figure 8.** STM image of the  $(2\sqrt{3} \times 2\sqrt{3})R30^\circ$  superstructure showing the rotation shift of the average orientation resulting from local defects between perfect domains. Highlighted the domains and the defects. ( $V = -1.7V, I = 1.1nA$ )

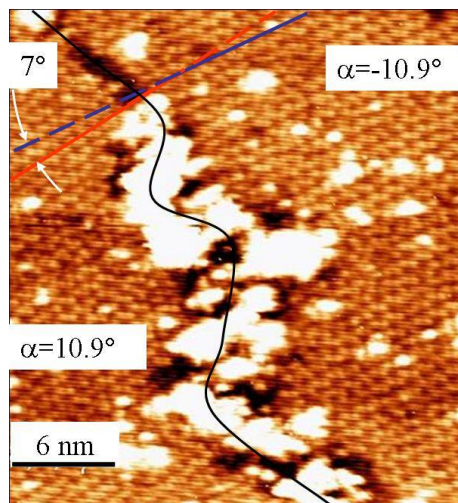


**Figure 9.** STM image showing two  $(2\sqrt{3} \times 2\sqrt{3})R30^\circ$  domains with local defects giving rise to a grain boundary ( $V = -2.0V, I = 900pA$ )

## 8. Conclusion

In this paper we have shown each one of the five superstructures of silicene on silver (111): the  $(4 \times 4)$ , the two different  $(\sqrt{13} \times \sqrt{13})R13.9^\circ$ , the  $(2\sqrt{3} \times 2\sqrt{3})R30^\circ$  and the  $(\sqrt{7} \times \sqrt{7})R19.1^\circ$ . We explained the LEED and STM observations by ball models. In the case of the  $(2\sqrt{3} \times 2\sqrt{3})R30^\circ$  superstructure, we show that local defects located around perfect  $(2\sqrt{3} \times 2\sqrt{3})R30^\circ$  areas justify the average orientation shift observed in the  $(2\sqrt{3} \times 2\sqrt{3})R30^\circ$ .

## References

- [1] Léandri C, Oughaddou H, Aufray B, Gay J.M., Le Lay G, Ranguis A et al 2007 *Surface Science*. **601** 262
- [2] Aufray B, Kara A, Vizzini S, Oughaddou H, Léandri C, Ealet B and Le Lay G 2010 *App. Phys. Lett.* **96** 183102
- [3] Lalmi B, Oughaddou H, Enriquez H, Kara A, Vizzini S, Ealet B and Aufray B 2010 *Appl. Phys. Lett.* **97** 223109
- [4] Kara A, Enriquez H, Seitsonen A.P, Lew Yan Voon, L.C, Vizzini S, Aufray B et al 2012 *Surface Science Reports* **67** 1
- [5] Feng B, Ding Z, Meng S, Yao Y, He X, Cheng P, Chen L and Wu K 2012 *Nano Lett.* **12** 3507
- [6] Jamgotchian H, Colignon Y, Hamzaoui N, Ealet B, Hoarau J Y, Aufray B and Bibérian J P 2012 *J. Phys. Cond. Mat.* **24** 172001

- [7] Lin C, Arafune R, Kawahara K, Tsukahara N, Minamitani E, Kim Y, Takagi N and Kawai M 2012 *App. Phys. Exp.* **5** 045802
- [8] Vogt P, De Padova P, Quaresima C, Avila J, Frantzeskakis E, Asensio M.C et al 2012 *Phys. Rev. Lett.* **108** 155501
- [9] Arafune R, Lin C-L, Kawahara K, Tsukahara N, Minamitani E, Kim Y et al 2013 *Surf. Sci.* **608** 297
- [10] Chen L, Liu C-C, Feng B, He X, Cheng P, Ding Z et al 2012 *Phys. Rev. Lett.* **109** 056804
- [11] Chiappe D, Grazianetti C, Tallarida G, Fanciulli M and Molle A 2012 *Advanced Materials* **24** 5088
- [12] Enriquez H, Vizzini S, Kara A, Lalmi B and Oughaddou H 2012 *J. Phys. Condens. Matter* **24** 314211
- [13] Gao J and Zhao J 2012 *Sci. Rep.* **2** 861
- [14] Kaltsas D, Tsetseris L and Dimoulas A 2012 *J. Phys. Condens. Matter* **24** 442001
- [15] Perdereau J and Rhead G.E 1971 *Surf. Sci.* **24** 555